Ultralow-n SiO₂ Thin Films Synthesized Using Organic Nanoparticles Template

Mai Xuan Dung, June Key Lee,[†] Woo-Sik Soun,[‡] and Hyun-Dam Jeong[*]

Department of Chemistry and Institute of Basic Science, Chonnam National University, Gwangju 500-757, Korea
[*]E-mail: hdjeong@chonnam.ac.kr
[†]Department of Materials Science and Engineering, Chonnam National University, Gwangju 500-757, Korea
[‡]New Technology and Analysis Department, National Nanofab Center, Daejeon 305-806, Korea
Received September 16, 2010, Accepted September 30, 2010

In an original effort, this lab attempted to employ polystyrene nanoparticles as a template for the synthesis of ordered and highly porous macroporous SiO₂ thin films, utilizing their high combustion temperature and narrow size distribution. However, polystyrene nanoparticle thin films were not obtained due to the low interaction between individual particles and between the particle and silicon substrate. However, polystyrene-polyacrylic acid (PS-AA) colloidal particles of a core-shell structure were synthesized by a one-pot miniemulsion polymerization approach, with hydrophilic polyacrylic acid tails on the particle surface that improved interaction between individual particles and between the particle and silicon substrate. The PS-AA thin films were spin-coated in the thickness ranges from monolayer to approximately 1.0 μm. Using the PS-AA thin films as sacrificial templates, macroporous SiO₂ thin films were successfully synthesized by vapor deposition or conventional solution sol-gel infiltration methods. Inspection with field emission scanning electron microscopy (FE-SEM) showed that the macroporous SiO₂ thin films consist of interconnected air balls (~100 nm). Typical macroporous SiO₂ thin films showed ultralow refractive indices ranging from 1.098 to 1.138 at 633 nm, according to the infiltration conditions, which were confirmed by spectroscopy ellipsometry (SE) measurements. This research shows how the synthetic control of the macromolecule such as hydrophilic polystyrene nanopaticles and silicate sol precursors innovates the optical properties and processabilities for actual applications.

Key Words: Ultralow-n, Macroporous, SiO₂, Polystyrene nanoparticles, Template thin films

Introduction

Refractive index (denoted as n) is one of the most important properties of a material since it is related to how much the material interacts with light. As a light beam travels from medium 1 to medium 2, it is partially reflected back to medium 1 and refracted into medium 2 at the interface, as schematically drawn in Fig. 1.

The reflectivity of light is mathematically expressed by Fresnel's equations:

$$r_{12}^p = \frac{N_2 \cos\varphi_1 - N_1 \cos\varphi_2}{N_2 \cos\varphi_1 + N_1 \cos\varphi_2} \; ;$$
$$r_{12}^s = \frac{N_1 \cos\varphi_1 - N_2 \cos\varphi_2}{N_1 \cos\varphi_1 + N_2 \cos\varphi_2}$$

(Eq. 1)

Where, $N_1 \sin\varphi_1 = N_2 \sin\varphi_2$, r^p, r^s, N_1, N_2, φ_1, φ_2 are the reflectivities of p-wave, s-wave components, complex refractive indices of media 1 and 2, and the incident and refractive angles, respectively. The reflectance of light at a normal incidence ($\varphi_1 = 0°$) at the boundary between two dielectric media is a real number:

$$R^p = (r^p)^2 = \left(\frac{n_2 - 1}{n_2 + 1}\right)^2 = (r^s)^2 = R^s$$

(Eq. 2)

In the case of common glass, with a refractive index of 1.52 at 633 nm, the reflectance at the air-glass interface is ~0.0426,
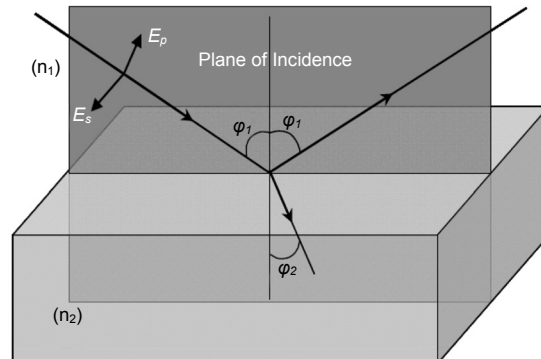

Figure 1. The reflection and refraction of light at the interface between medium 1 and 2. φ_1, φ_2, n_1, n_2, E_p, and E_s are incident angle, refraction angle, refractive indices of medium 1 and medium 2, amplitudes of electric field waves parallel or perpendicular to plane of incidence, respectively. The plane of incidence refers to the plane containing incoming light, reflecting light and lying perpendicular to the interface.

implying that 95.74% of the light is transmitted into the glass.

To improve the transmittance of light from a medium of index n_1 to a medium of index n_2, a thin film needs to lie between them. A single layer with a refractive index of the root square of the product of n_1 and n_2, and whose thickness is a quarter wavelength (λ/4), is optimal for the transmittance of the single wavelength (λ) at a normal incidence ($\varphi = 0°$). In addition, a graded refractive index film consisting of several layers whose refractive indices are stepwise increasing from n_1 to n_2, accompanied with a controlled thicknesses, is able to eliminate light reflection over a wide range of incident angles.[1,2] As air or vacuum is usually

considered one of the media, a material with a refractive index close to 1.00 is thought to be required to construct high-performance anti-reflection films.

Furthermore, the availability of ultralow refractive index (ultralow-n) materials allow construction of not only low loss glasses,[3] but also many excellent optical devices[4] such as internal omni-directional reflectors,[5] distributed Bragg reflectors (DBRs),[6] and waveguides.[7] However, dense materials with a refractive index close to 1.0 do not actually exist. Select available materials not unlike SiO_2 and MgF_2 have refractive indices near 1.4, which are not sufficiently low for the graded-index coating. Since the refractive index of a dielectric material is directly proportional to its density, and silicon oxide (SiO_2) is transparent in the UV-visible range, ultralow-n thin films are usually fabricated in highly porous SiO_2 thin films. Schubert's group demonstrated a very low refractive index (1.05 at 632.8 nm) material consisting of SiO_2 nanorods fabricated by an oblique-angle electron-beam deposition method,[8] which was later found to be inapplicable towards large scale production because low pressure and controlled partial oxygen pressure conditions are required. Recently, Yamaguchi *et al.* synthesized thin films of mesoporous nanoparticles by a solution templating process, showing a refractive index ranging from 1.07 to 1.16.[9] These values are lower than that of conventional mesoporous silicon oxides (near 1.2) or meso-macro hierarchical films (near 1.14), which were also obtained by the solution process.[10] However, not only is the templating process sensitive to environmental conditions (temperature and humidity) and chemical composition (silicon resources, surfactants, solvents),[11] but the optical properties of the resultant mesoporous thin films are gradually degraded due to strong moisture adsorption.[12] A colloidal template-based method, on the contrary, is stable to various inorganic precursors and is primarily used to synthesize macroporous materials.[13] This method includes three discrete steps: 1) synthesis of a closely packed template of organic colloidal nanoparticles such as polystyrene (PS) or poly(methyl methacrylate); 2) infiltration of the voids within the template of the colloidal nanoparticles with an inorganic precursor, followed by solidification; 3) removal of the organic template either by calcination or extraction, leaving air balls with sizes defined from the organic templating particles. This method has been used extensively to synthesize ordered macrostructures of various materials.[14] Unfortunately, the convective vertical deposition method that has been primarily used to form colloidal nanoparticle films requires a very long period of time. In addition, the colloidal nanoparticle thin films have a small uniform area, several micrometer square domains, and are also macroscopically changing in film thickness along the withdrawing direction. This imperfect colloidal nanoparticle thin film is mainly due to a lack of

controllability in process factors such as solvent (water in most cases) evaporation rate, which is required for maintaining the concentration of the colloidal solution and wetting ability of the colloidal solution upon the substrate surface.[15] In the case of PS, the low interaction between the particles and between the particle and substrate was attributed mainly to van der Waals interactions. In addition, the crystallization of PS particles is slow as growth of the template crystal driven by the capillary force is opposed by Brownian motion. In the opinion of the authors, by modifying the surface of the PS particles with an electrolyte polymer such as polyacrylic acid (AA), not only will strong interaction between particles be added by electrostatic forces, but also the wetting ability of the colloidal solution on the substrate surface could be enhanced. Eventually, the colloidal nanoparticle thin films (CNFs) can be synthesized by much faster methods such as spin- or dip-coating. Herein, we report the use of polystyrene-polyacrylic acid nanoparticles (PS-AA) synthesized by a one-pot miniemulsion polymerization approach[16] as a template for the synthesis of macroporous SiO_2 thin films of an ultralow-n.

Experimental Section

Synthesis of polystyrene/polyacrylic acid nanoparticles. Styrene (St) and acrylic acid (AA) (Sigma-Aldrich, St. Louis, MO, USA) were distilled under diminished pressure to remove inhibitor reagents and stored in a refrigerator prior to use. An oil phase including styrene, acrylic acid, hexadecane (HD) (Sigma-Aldrich), and oil-soluble initiator 2,2'-azobisisobutyronitrile (V-59) (Dejung Chemicals & Metals. Co. Ltd, Shiheung, Gyeonggi-do, South Korea) was prepared in a 20 mL vial in an ice-bath and stirred with a magnetic stirrer. The water phase, including distilled water and cetyltrimethylammonium bromide (CTAB) (Sigma-Aldrich), was prepared separately in a 250 mL flask equipped with a mechanical stirrer.

The chemical composition is given in Table 1. After achieving a transparent oil solution, it was injected into the flask. The mixture was stirred at 300 rpm for 1 h before treatment in an ultrasonic bath (Branson 2510) for 20 min to produce a miniemulsion system. The flask was then placed in a hot oil bath kept at 70 $^\circ$C by a heater controller (± 1 $^\circ$C accuracy) and the mixture stirred at 300 rpm with a mechanical stirrer. The polymer reaction took place for 24 h per run. Particle size distribution was analyzed with a surface zeta potential & particle size analyzer (Otsuka Electronics, ELS-8000, Hirakata-shi, Osaka, Japan). Samples were prepared by repeated centrifugation (12000 rpm for 30 min) and re-dispersion in water four times to remove the remaining unreacted reagents and surfactant CTAB.

Synthesis of template thin films of nanoparticles (TF). Solu-

Table 1. Recipe for miniemulsion polymerization reactions and properties of polystyrene/polyacrylic acid nanoparticles.

	Oil phase				Water phase		Nanoparticles properties	
	St (g)	AA (g)	HD (g)	V-59 (g)	Water (g)	CTAB (g)	Aver size (nm)	Pol-dis (%)
PS	6	0	0.25	0.1	24	0.13	109.7	9.3
PS-5AA	5.7	0.3	0.25	0.1	24	0.13	88.2	15.9
PS-10AA	5.4	0.6	0.25	0.1	24	0.13	88.9	16.7

tions of polystyrene (PS) and polystyrene/polyacrylic acid (5 and 10% wt) (PS-5AA, PS-10AA) in water, with concentrations ranging from 1 to 15 wt %, were prepared from the mother solution obtained after polymerization at a concentration ~ 18 wt %. A hydrophilic silicon wafer was made by treatment with piranha solution (70% volume of concentrated H_2SO_4 (98 wt %) and 30% volume H_2O_2 (30 wt % in water)) at 80 ^{o}C for 30 min, followed by full, sequential cleaning in distilled water, ethanol, and acetone, and dried in a nitrogen flow. Nanoparticle thin films were made by a spin-coating method with a spin-coater Midas SP-IN 1200 (Korean), which included two steps: a wetting step (500 rpm for 5 s); a flatting step (2000 rpm for 25 s). Some alternative samples were fabricated using 1500 or 1000 rpm in the second step to achieve thicker films. As-prepared thin films were then put on the bottom of a beaker and transferred in an ultrasonic bath for 30 min.

Microscopic pictures of the template thin film were taken with an Olympus Sz61 camera. Thicknesses of the template thin films were determined from field emission scanning electron microscope (FE-SEM) images.

Synthesis of macroporous SiO₂ thin films. The air voids within the template thin films were filled by either vapor deposition or soaking methods. In the vapor deposition method, template films were taped on the bottom of a 250 mL beaker, which was then placed reversely on a glass plate. Two separate vials containing tetraethylorthosilicate (TEOS) (Sigma-Aldrich) and HCl 20 wt % solution, respectively, were placed onto the glass, inside the beaker, and then transferred into an oven and kept at 90 ^{o}C. After a designated amount of time, the films were taken out and transferred to a furnace for further calcination. In the soaking method, vacuum dried template films were soaked for 3 min in the sol solutions which had been already prepared from TEOS, HCl, water, and ethanol at a molar ratio of :0.13:5:20.
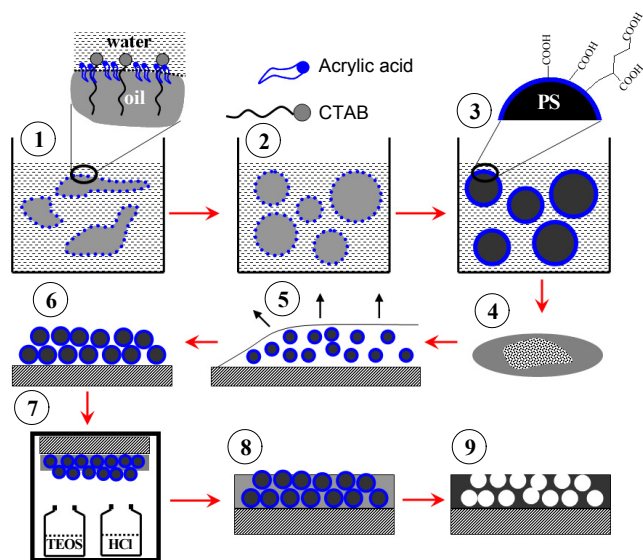
The over layer of the solution upon the film was spun out at 3000 rpm for 10 s. Films were further cured overnight under room conditions prior to calcination. Calcination was carried out at 500 ^{o}C for 4 h (4 ^{o}C per min) to remove the polymer template. The overall scheme of the experiment is illustrated in Fig. 2.

The FE-SEM technique was performed with a JSM-7500F (JEOL, Akishima, Tokyo, Japan), operated at 15 kV. The Pt coating was applied to all samples before FE-SEM measurements. Refractive indices of macroporous thin films were obtained from spectroscopic ellipsometry (SE) measurements on M2000D (J. A. Wollam Co. Inc., Suite, Lincoln, USA), at wavelengths ranging from 200 to 1000 nm.

One sample of the macroporous SiO₂ thin films on glass was prepared by a vapor deposition procedure to confirm the loss of light accounted by scattering at the macroporous layer. Ultraviolet visible (UV-vis) absorption spectroscopy was performed within a range of 200 - 1200 nm on a SCINCO S-3150.

Results and Discussion

Properties of colloidal nanoparticles (PS, PS-5AA, PS-10AA) whose respective polyacrylic acid weight percentages were 0, 5, and 10% are given in Table 1 and Fig. 3. All PS-AA particles obtained by the miniemulsion polymerization method using an oil soluble initiator possessed a "hairy" structure in which hydrophilic polyacrylic acid tails were outside the spherical polystyrene core; increase in the polydispersity index and bimodal size distribution features occurred simultaneously when acrylic acid was added to the oil phase.[17] The synthesis and structure of the PS-AA particles are schematically illustrated as the first portion in Fig. 2.

The formation of the template film includes two steps: a flat layer of colloidal solution is coated, driven by centrifugal force; the nanoparticle self-assembly is induced by the capillary force as the water evaporates. Figure 4 shows the micrograph of the template films obtained by spin-coating colloidal solutions on either untreated (**a**) or piranha-treated silicon wafers (**b**). The PS solution was poorly coated onto the untreated wafer over a wide range of concentrations from 1 to 15 wt % (Fig. 4a), and
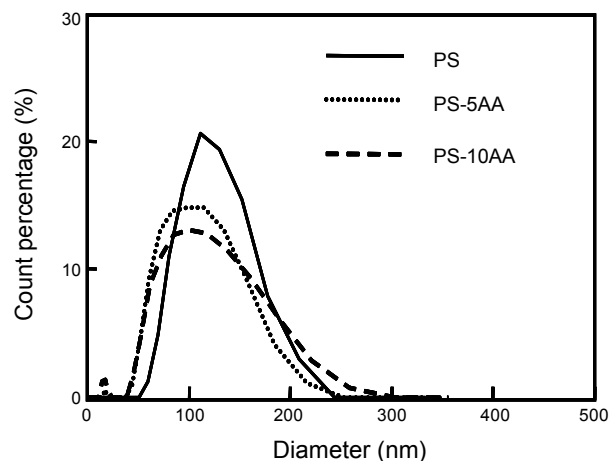
Figure 2. Schematic of experimental sequence. 1) Emulsion preparation; 2) Formation of miniemulsion system induced by ultrasonic vibration; 3) Colloidal solution after polymer reaction; 4) Spin-coating; 5) Wet film of latex solution; 6) Dried template thin film; 7) Vapor deposition setup; 8) As-prepared SiO₂ film; 9) Macroporous SiO₂ film after calcination.

Figure 3. Size distribution of PS, PS-5AA, and PS-10AA colloidal particles.
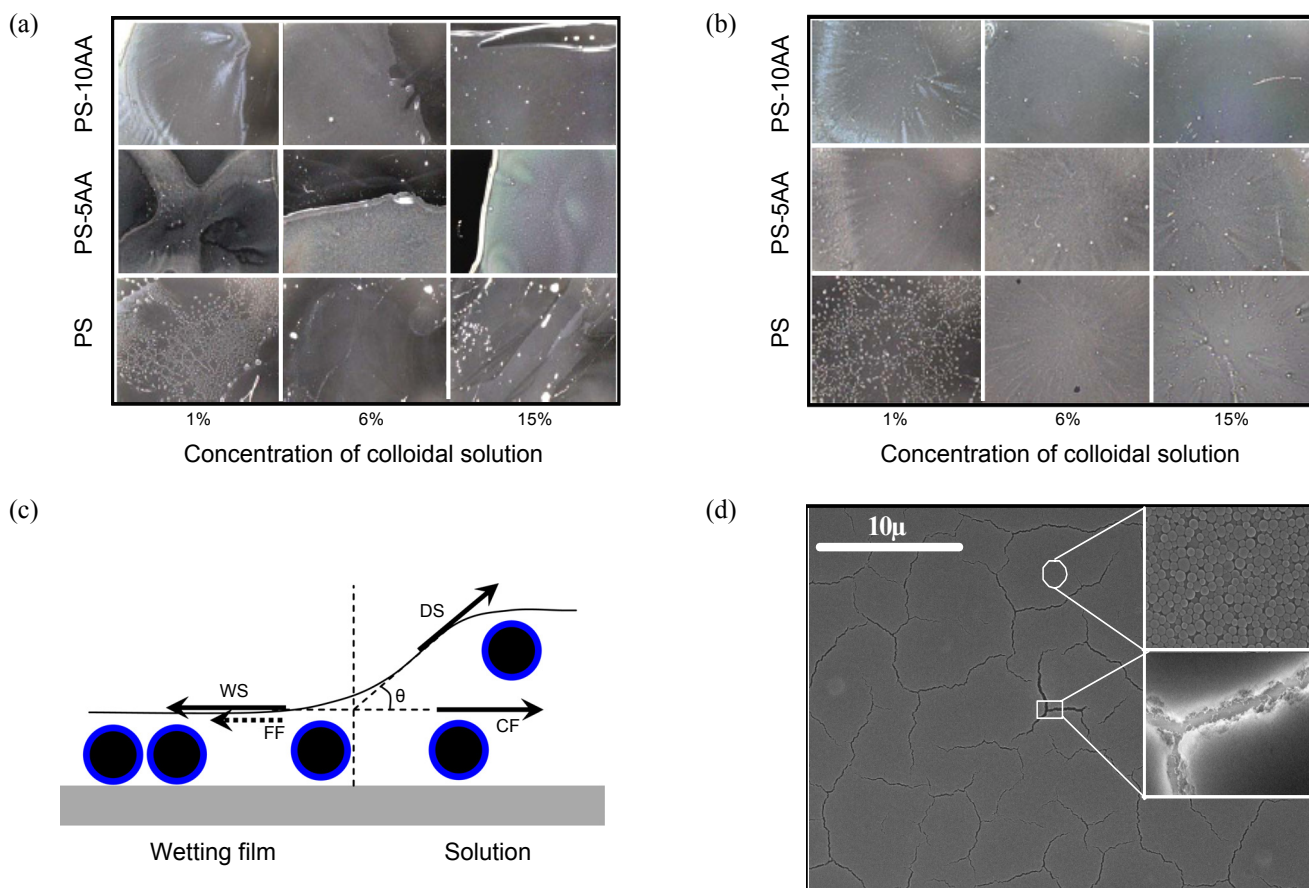
(a)

(b)

(c)

(d)

Figure 4. Micrographs of template films on untreated (a) and piranha-treated (b) silicon wafers. (c) Modified slip motion model explanation of template film formation. (d) Surface FE-SEM images of the template thin film obtained from the PS-10AA (9 wt %) solution at different magnification shows a less ordered structure (above) and empty cracks (below).

fully coated on the treated substrate by increasing its concentration higher than 6 wt % (Fig. 4b). Conversely, the PS-5AA or PS-10AA precursor solutions were partially coated on the untreated substrate (Fig. 4a) and fully coated on the piranha-treated silicon wafers (Fig. 4b).

In order to explain the various features of the templating films, the lab first supposed that solvent evaporation occurred after the wetting film was formed, which is reasonable because of the short time requirement of spin-coating step (30 s) and the high boiling point of water (100 °C). The differences between the templating films features mentioned above could be explained in more detail, based on a slip motion mechanism,[18] as illustrated in Fig. 4c. At the contacting line which is drawn by the dash line, the surface tension of the wetting film (WS) and the friction force (FF) tend to prevent the solution from slipping off the substrate and are in competition with droplet surface tension (DS) and centrifugal force (CF), both of which tend to drive the solution away. When the hydrophilicity of the substrate increases by treatment with the piranha solution, the friction force (FF) becomes greater, such that the solution state is more preferable on the substrate during spinning. As you can see in Fig. 4b, a random white dots feature was observed in the sample obtained from the 1 wt % PS solution on the hydrophilic wafer, due to the formation of droplets driven by the droplet surface

tension (DS), as water evaporated. This is because that, in this case, the surface tension (WS) and friction force (FF) which originates from the viscosity of the solution and the interaction between the particles and substrate surface, respectively, are insufficient. Additionally, in all cases, as the concentration of the colloidal solution increases, the morphology of the template film seems to be improved because of the decrease in droplet surface tension, together with the increase in frictional force induced by a thicker wetting layer.[15] It is worth mentioning that the template film quality was enhanced by using PS-AA colloidal solutions instead of PS ones. This may be due to the fact that the water-soluble polyacrylic acid tails of the PS-AA made the colloidal solution more viscous and that the interaction between the particle-particle and particle-substrate were improved, where the frictional force and wetting surface tension were both increased, keeping a flat wetting layer from droplet formation. In this report, PS-10AA was used for further investigation.

The topology of the dried template film is given in Fig. 4d, taken from the sample that used the PS-10AA 9 wt % solution on the hydrophilic silicon wafer. This includes micrometer domains and hexagonal cracks. During the drying process, water between the PS-10AA particles evaporated, producing a capillary force that in turn pulled particles closer together into a closely packed fashion.[15] Colloidal particles can be slipped over
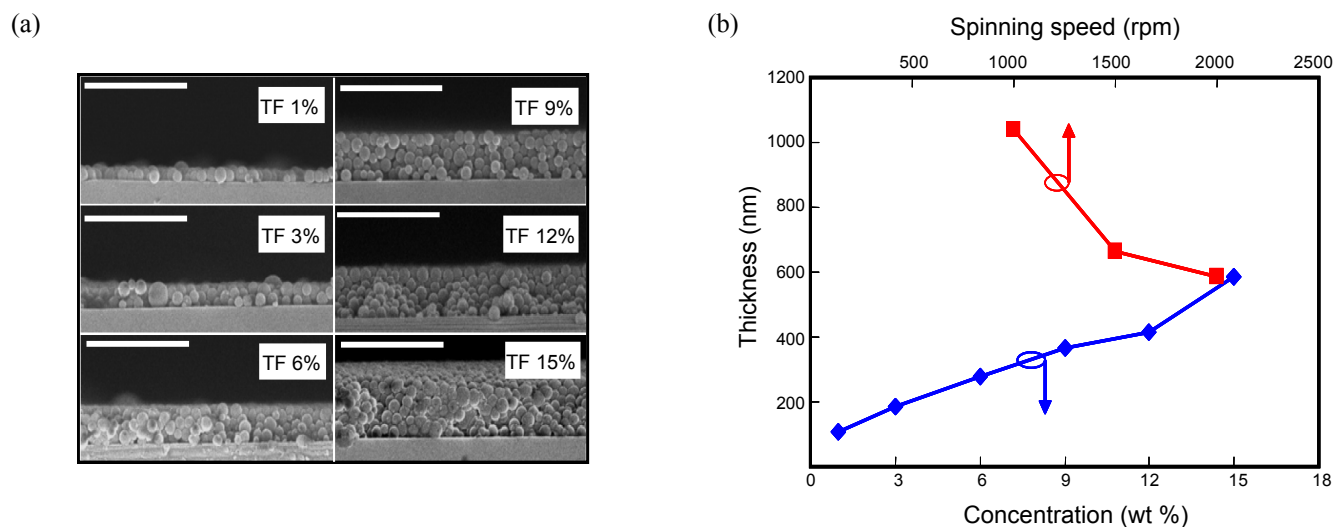
(a)

(b)

Figure 5. (a) Cross view FE-SEM images of template films assigned as TF (template thin films of nanoparticles) 1%, TF 3%, TF 6%, TF 9%, TF 12%, and TF 15% prepared from various colloidal solutions of PS-10AA in water with weight concentrations of 1 wt %, 3 wt %, 6 wt %, 9 wt %, 12 wt %, and 15 wt %, respectively. (b) Thickness of template thin films *vs.* weight concentration of colloidal solutions of PS-10AA in water (blue line) and *vs.* coating speed (red line). The bar scale in (a) is 1 μm. The PS-10AA solution of 15 wt % was used to make thicker TF by decreasing spinning speed (red line). Spinning speed of 2000 rpm was applied to make thicker TF by increasing weight concentrations of the PS-10AA solutions (blue line).
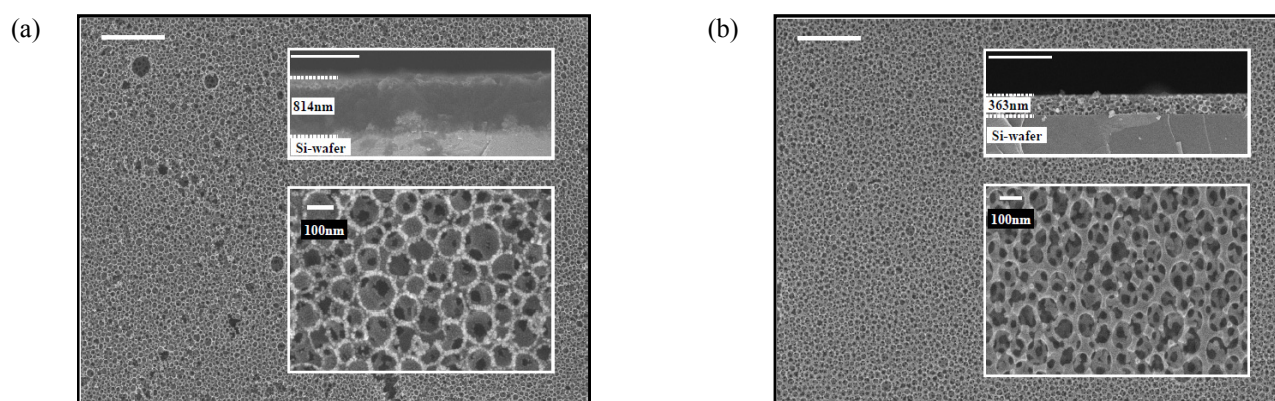
(a)

(b)

Figure 6. FE-SEM images of macroporous SiO₂ thin films obtained by the soaking method (a) and vapor deposition method with 1 h of exposure time (b). Scaling bar is 1.0 μm. Inserted FE-SEM pictures are cross view (above) and surface view at higher magnification for each sample (below).

the substrate by capillary forces so that empty cracks are formed, as shown in Fig. 4d. The template film consisted of loosely packed particles (Fig. 4d) due to the high polydispersity index PS-10AA nanoparticles used.[19] The high friction between the PS-10AA particles and hydrophilic substrate diminished the action of the capillary force onto the particles and into a well organized arrangement. Another possible reason accounting for the less ordered template film structure is fast evaporation of water in the film type, compared to traditional convective vertical deposition.

Cross-section FE-SEM images (Fig. 5a) confirm formation of a flat template thin film of PS-10AA from different solutions. The thickness of the template film was linear in proportion to the concentration of the PS-10AA solution, or reciprocal speed of the second coating step (Fig. 5b), and can be tuned in a wide range from near 100 nm to approximately 1.0 μm.
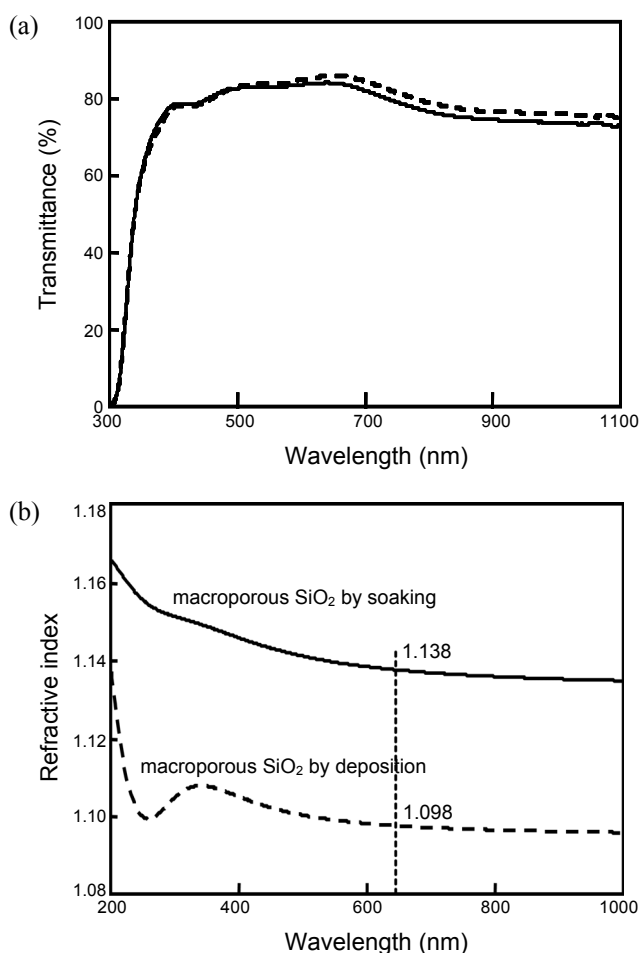
It has been reported that the template film of the polystyrene

nanoparticle (PS) readily falls off from the substrate when immersed into ethanolic solution of metal alkoxide because of the weak interactions between the PS film and substrate.[20] As discussed earlier, the polyacrylic acid chains on the surface of the PS could enhance this interaction such that the thin films are thought to be capable of withstanding the ethanolic solution. This lab employed template films made of PS-10AA with different thickness, as shown in Fig. 5, in order to infiltrate the voids within the template films by the conventional sol-gel process (denoted the soaking method, see Experimental Section). Unfortunately, one of these films whose thickness neared 1.0 μm, was maintained after soaking in an ethanolic sol solution of TEOS. The corresponding SiO₂ film obtained after removing the PS-10AA template is shown in Fig. 6a. Evidently, a flat macroporous SiO₂ film consisting of interconnected air balls was formed.

Due to slipping problems, a vapor deposition method was

3598   *Bull. Korean Chem. Soc.* **2010**, Vol. 31, No. 12

Mai Xuan Dung et al.

Table 2. Thicknesses and surface properties of macroporous SiO₂ thin films obtained by the vapor deposition method.

	TF thickness (nm)	Exposing time (minutes)	SiO₂ films	
			Thickness (nm)	Surface
MF 1%	107	30	98	Rough
MF 3%	183	40	-	Rough
MF 6%	276	50	179	Rough
MF 9%	365	60	363	Smooth
MF 12%	416	70	351	Rough
MF 15%	583	80	557	Smooth

Figure 7. (a) Transmittance of uncoated glass (solid line) and glass coated with ~360 nm thick macroporous SiO₂ (dashed line). (b) Refractive index *vs.* wavelength of macroporous SiO₂ films obtained by different methods.

employed in lieu of a soaking method for thinner template films, schematically shown in Fig. 2. Properties of the resultant macroporous SiO₂ films are summarized in Table 2. Surface quality of the SiO₂ films changed contingently; rough films resulted from the thickness of the macroporous thin films being much lower than that of the corresponding template film. Within the experimental conditions, the low controllability of the vapor flow or the insufficient exposure time could be the source of the bad SiO₂ films. Logically, the thickness of the resultant SiO₂ films

could reach that of the corresponding template film. If the flow of the reagents vapor is under control, a flat SiO₂ can be produced, as was observed in the macroporous thin film at 9%. The FE-SEM images for the 9% are shown in Fig. 6b, where it is clear that a flat macroporous SiO₂ film over a large area consists of interconnected air balls of a size of approximately 90 nm.

The macropores of the SiO₂ film of a size of approximately 90 nm were directly obtained from the PS-10AA template nanoparticles after calcination. These values were much smaller than the wavelength of light in the visible range (> 400 nm), ensuring a low loss of light due to scattering. As shown in Fig. 7a, transmittance of coated glass fabricated by the same procedure as described for silicon substrates was slightly higher than that of uncoated glass.

Macroporous thin films possess very low refractive indices over a wide range, from visible to near infrared radiation, Fig. 7b. Refractive indices at 633 nm of the films obtained by soaking and vapor deposition methods were 1.138 and 1.098, respectively. From the Lorentz-Lorenz effective medium approximation equation:[21]

$$f = 1 - \left[\frac{n_{eff}^2 - 1}{n_{eff}^2 + 2} \right] / \left[\frac{n_{sil}^2 - 1}{n_{sil}^2 + 2} \right] \qquad \text{(Eq. 3)}$$

where f, n_{eff}, and n_{sil} are volume fraction of air (n = 1) or porosity of film and refractive indices of porous SiO₂ film and dense SiO₂ (n = 1.460), respectively. Therefore, the porosities of the macroporous films were calculated at 67.3 and 76.6%, respectively. These values are close to that of ordered macroporous SiO₂ (74%) film fabricated from a closely packed colloidal template.[14,15] Since the sacrificial template films used for the synthesis of macroporous SiO₂ are less ordered, their high porosities here are likely to result in part from other resources. While in the first film, its porosity partially caused the removal of organic moieties during thermal treatment, the extremely high porosity of the second film was due to its hollow structure in which secondary voids exist among hollows.[20]

Conclusions

The addition of hydrophilic polyacrylic acid onto the surface of the polystyrene nanoparticles improved the formation of template thin films of high quality from the spin-coating process, in which an increase in the interaction between colloidal particles and the hydrophilic substrate plays an important role. The thin films of the polystyrene/polyacrylic acid nanoparticles had a less ordered structure and their thickness was well controlled over a wide range by changing concentrations of the colloidal solution or spin-coating speed. Using these colloidal templates, macroporous SiO₂ thin films with thicknesses varying from hundreds of nanometers to micrometers were fabricated using either soaking or vapor deposition methods. Both types of the resultant films consisted of interconnected air voids of sizes near 90 nm. The film obtained from the soaking method had a refractive index of 1.138, whereas fabricated by the vapor deposition method showed an even lower value of 1.098 at 633 nm.

Our ultralow-n materials are very unique for its applicability into not only low loss glasses, but also many excellent optical devices such as internal omni-directional reflectors, distributed Bragg reflectors (DBRs), and waveguides. Moreover, they are highly impacting due to their low-cost, large area, and solution processability. This research shows how the synthetic control of the macromolecule such as hydrophilic polystyrene nanoparticles and silicate sol precursors innovates the optical properties and processabilities for actual applications.

References

1. Křepelka, J. I. *Jemná Mechanika A Optika.* **1992**, *3*, 53.
2. Dobrowolski, J. A.; Poitras, D.; Ma, P.; Valkil, H.; Acree, M. *Appl Optics.* **2002**, *41*, 3075.
3. Xi, J.-Q.; Schubert, M. F.; Kim, J. K.; Schubert, E. F.; Chen, M.; Lin, S.-Y.; Liu, W.; Smart, J. A. *Nat. Photonics.* **2007**, *1*, 176.
4. Schubert, E. F.; Kim, J. K.; Xi, J.-Q. *Phys. Stat. Sol. B* **2007**, *244*, 3002.
5. Xi, J.-Q.; Ojha, M.; Plawsky, J. L.; Gill, W. N.; Kim, J. K.; Schubert, E. F. *Appl. Phys. Lett.* **2005**, *87*, 031111.
6. Xi, J.-Q.; Kim, J. K.; Schubert, E. F. *Nano Lett.* **2005**, *5*, 1385.
7. Konjhodzic, D.; Schröter, S.; Marlow, F. *Phys. Stat. Sol. A* **2007**, *204*, 3676.
8. Xi, J.-Q.; Kim, J. K.; Schubert, E. F.; Ye, D.; Lu, T.-M.; Lin, S.-Y. *Opt. Lett.* **2006**, *31*, 601.
9. Yamaguchi, M.; Nakayama, H.; Yamada, K.; Imai, H. *Opt. Lett.* **2009**, *34*, 2060.
10. Falcaro, P.; Malfatti, L.; Kidchob, T.; Giannini, G.; Falqui, A.; Casula, M. F.; Amenitsch, H.; Marmiroli, B.; Grenci, G.; Innocenzi, P. *Chem. Mater.* **2009**, *21*, 2055.
11. Grosso, D.; Cagnol, F.; Soler-Illia, G. J. de A. A.; Crepaldi, E. L.; Amenitsch, H.; Brunet-Bruneau, A.; Bourgeois, A.; Sanchez, C. *Adv. Funct. Mater.* **2004**, *14*, 309.
12. Pénard, A.-L.; Gacoin, T.; Boilot, J.-P. *Acc. Chem. Res.* **2007**, *40*, 895.
13. Holland, B. T.; Blanford, C. F.; Stein, A. *Science* **1998**, *281*, 538.
14. Xia, B. Y.; Gates, B.; Yin, Y.; Lu, Y. *Adv. Mater.* **2000**, *12*, 693.
15. Teh, L. K.; Tan, N. K.; Wong, C. C.; Li, S. *Appl. Phys. A* **2005**, *81*, 1399.
16. Landfester, K. *Macromol. Rapid Commun.* **2001**, *22*, 896.
17. Musyanovych, A.; Rossmanith, R.; Tontsch, C.; Landfester, K. *Langmuir* **2007**, *23*, 5367.
18. Adachi, E.; Dimitrov, A. S.; Nagayama, K. *Langmuir* **1995**, *11*, 1057.
19. Micheletto, R.; Fukuda, H.; Ohtsu, M. *Langmuir* **1995**, *11*, 3333.
20. Li, Y.; Kunitake, T.; Fujikawa, S. *Colloids Surf. A* **2006**, *275*, 209.
21. Himcinschi, C.; Friedrich, M.; Frühauf, S.; Streiter, I.; Schulz, S. E.; Gessner, T.; Baklanov, M. R.; Mogilnikov, K. P.; Zahn, D. R. T. *Anal. Bioanal. Chem.* **2002**, *374*, 654.